Table S1. X-ray data collection and refinement statistics

Data collection	SARS-CoV-2 wild-type RBD + HB148 + LY-CoV1404	SARS-CoV-2 wild-type RBD + HB148-M4 + LY-CoV1404	SARS-CoV-2 Omicron BA.1 RBD + HB148-M4 + LY-CoV1404
Beamline	NSLS-II 17-ID-2	SSRL BL12-1	SSRL BL12-1
Wavelength (Å)	0.97934	0.97946	0.97946
Space group	P1	C 1 2 1	C 1 2 1
Unit cell parameters			
a, b, c (Å)	85.3, 86.1, 98.8	195.8, 88.7, 99.9	196.8, 88.0, 100.8
α, β, γ (°)	115.7, 89.7, 94.4	90, 112.0, 90	90, 110.3, 90
Resolution (Å) [a]	50.0-3.10 (3.15-3.10)	50.0-2.60 (2.64-2.60)	50.0-2.73 (2.78-2.73)
Unique reflections [a]	45,996 (2,261)	47,927 (2,367)	42,283 (1,794)
Redundancy [a]	2.0 (1.9)	4.7 (3.1)	5.5 (3.3)
Completeness (%) [a]	97.8 (96.7)	98.0 (97.7)	96.5 (82.7)
$\langle I/\sigma_I \rangle$ [a]	4.3 (1.0)	15.4 (1.2)	14.7 (1.3)
R_{sym} [b] (%) [a]	17.6 (65.3)	11.5 (>100)	15.6 (>100)
R_{pim} [b] (%) [a]	15.2 (58.4)	5.7 (69.5)	6.8 (55.9)
$CC_{1/2}$ [c] (%) [a]	99.6 (40.3)	98.7 (58.8)	98.3 (68.8)
Refinement statistics			
Resolution (Å)	48.8-3.10	36.1-2.60	40.8-2.73
Reflections (work)	39,220	42,405	34,641
Reflections (test)	1,841	2,109	2,000
R_{cryst} [d] / R_{free} [e] (%)	21.3/25.9	19.3/24.3	20.0/25.3
Copies of Fab/RBD per ASU	2	1	1
No. of atoms	15,954	8,159	8,052
Fab	12,828	6,420	6,438
RBD	3,116	1,558	1,522
Ligands [f]	10	17	42
Water	0	156	50
Average *B*-values (Å^2)	69	50	50
Fab	70	51	51
RBD	65	49	48
Ligands [f]	75	51	54
Water	-	40	31
Wilson *B*-value (Å^2)	67	44	43
RMSD from ideal geometry			
Bond length (Å)	0.002	0.002	0.002
Bond angle (°)	0.50	0.55	0.52
Ramachandran statistics (%) [g]			
Favored	96.95	97.58	97.18
Outliers	0.05	0.00	0.00
PDB code	9ZBW	9ZBX	9ZBY

[a] Numbers in parentheses refer to the highest resolution shell.

[b] $R_{sym} = \Sigma_{hkl} \Sigma_i | I_{hkl,i} - \langle I_{hkl} \rangle | / \Sigma_{hkl} \Sigma_i I_{hkl,i}$ and $R_{pim} = \Sigma_{hkl} (1/(n-1))^{1/2} \Sigma_i | I_{hkl,i} - \langle I_{hkl} \rangle | / \Sigma_{hkl} \Sigma_i I_{hkl,i}$, where $I_{hkl,i}$ is the scaled intensity of the ith measurement of reflection h, k, l, $\langle I_{hkl} \rangle$ is the average intensity for that reflection, and *n* is the redundancy.

[c] $CC_{1/2}$ = Pearson correlation coefficient between two random half datasets.

[d] $R_{cryst} = \Sigma_{hkl} | F_o - F_c | / \Sigma_{hkl} | F_o |$ x 100, where F_o and F_c are the observed and calculated structure factors, respectively.

[e] R_{free} was calculated as for R_{cryst}, but on a test set comprising ~4.7%-5.8% of the data excluded from refinement.

[f] Bound ligands are phosphate, Tris(hydroxymethyl)aminomethane, and ethylene glycol molecules.

[g] From MolProbity.[1]

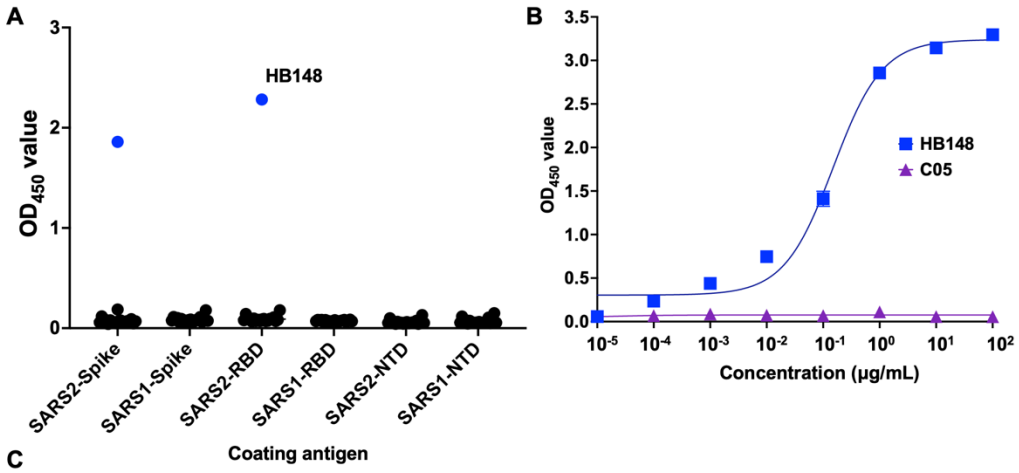

C

Antibody	IGHV	IGKV	CDR H3	CDR L3
HB148	*IGHV3-53*	*IGKV3-20*	CARDLFQVGATDYW	CQQYGSSPGYTF

Figure S1. Identification of human monoclonal antibodies to SARS-CoV-2 RBD. (A) The binding activity of 24 human monoclonal antibodies against full spike, RBD, NTD protein from SARS-CoV-1 and SARS-CoV-2 was measured by ELISA. **(B)** The binding affinity of HB148 (blue) IgG against SARS-CoV-2 RBD was measured by ELISA. C05 is an influenza hemagglutinin antibody and serves as a negative control here.[2] **(C)** Sequence information of antibody HB148 with heavy chain and light chain gene family and CDR3 amino acid sequence.

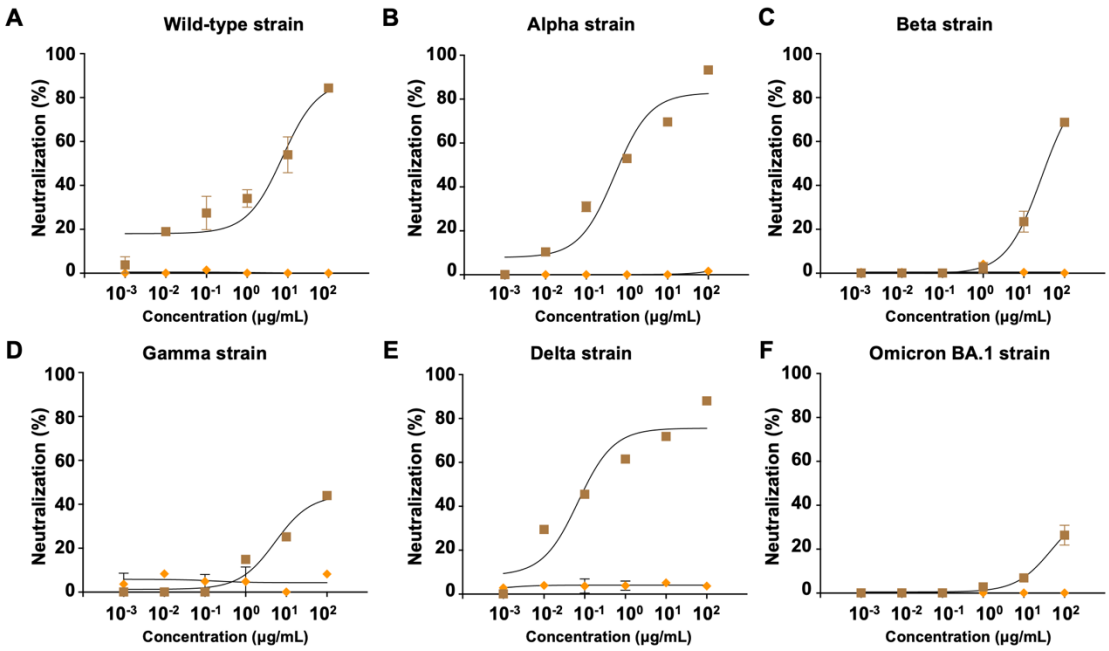

IC_{50}	Wild-type	Alpha	Beta	Gamma	Delta	Omicron BA.1
HB148	7.39	0.50	27.21	>100	20.90	>100
C05	>100	>100	>100	>100	>100	>100

Antibody NT_{50} (μg/mL)

Figure S2. Pseudovirus neutralizing ability of HB148 against different SARS-CoV-2 variants. Neutralization activity of antibody HB148 was determined by SARS-CoV-2 pseudovirus neutralization assay against **(A)** Wild-type strain, **(B)** Alpha strain, **(C)** Beta strain, **(D)** Gamma strain, **(E)** Delta strain and **(F)** Omicron BA.1 strain. Their estimated NT_{50} values are indicated. C05 is an influenza hemagglutinin antibody and serves as a negative control here.[2]

Figure S3. Sequence alignment of RBDs from different SARS-CoV-2 variants. Sequence alignment of RBD sequences from different SARS-CoV-2 variants was performed using MAFFT.[3] Conserved residues among wild-type and variant strains are highlighted in red, while residues that differ from the wild-type and may contribute to escape are highlighted in blue.

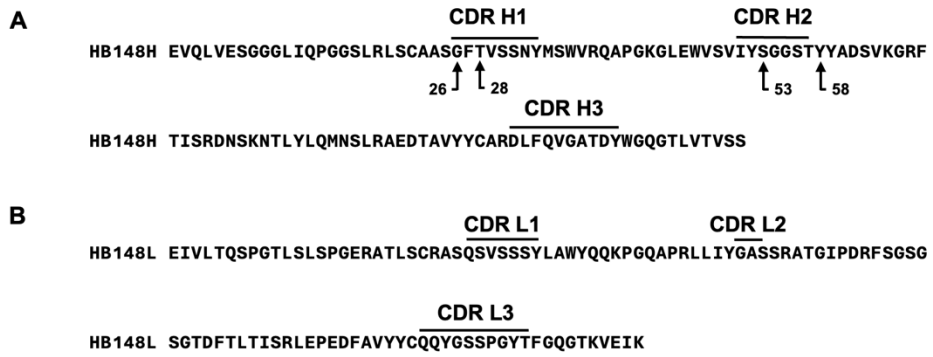

Figure S4. Amino acid sequence information for antibody HB148 with heavy chain and light chain CDR regions highlighted. CDR H1, CDR H2, CDR H3, and four potential somatic hypermutations in the HB148 heavy chain **(A)**, as well as CDR L1, CDR L2, and CDR L3 in the HB148 light chain **(B)**, were identified using IMGT.[4]

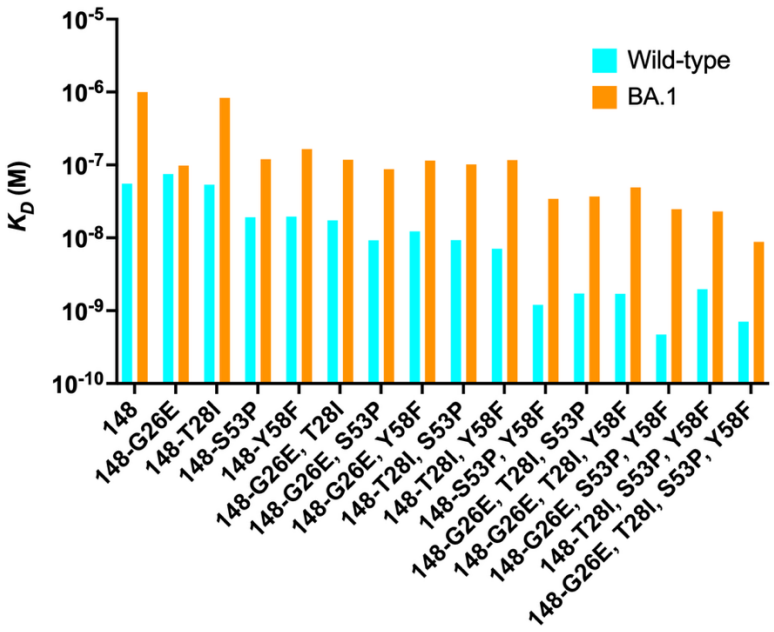

Figure S5. Binding affinity of HB148 WT and mutants against wild-type and Omicron BA.1 RBD. Binding kinetics of HB148 antibodies with different mutation combinations against wild-type RBD and Omicron BA.1 RBD were measured by biolayer interferometry (BLI). Y-axis represents the response.

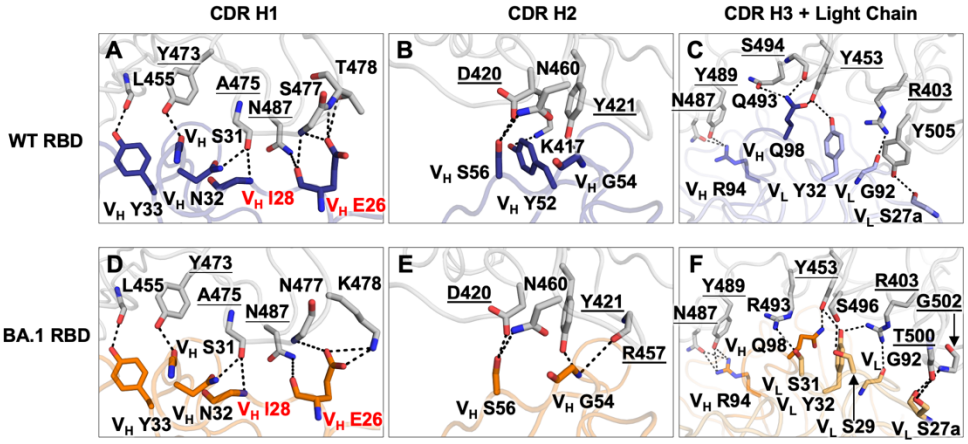

Figure S6. Crystal structure analysis of HB148-M4 with wild-type RBD and BA.1 RBD. Detailed molecular interactions (hydrogen bonds and salt bridges) of wild-type and BA.1 RBDs (grey backbone) with HB148-M4 are shown with V_H G26E and T28I labeled in red. Conserved epitope residues across VOCs are underlined.

SUPPLEMENTAL REFERENCES

1 Williams, C. J. *et al.* MolProbity: More and better reference data for improved all-atom structure validation. *Protein Sci* **27**, 293-315 (2018). https://doi.org/10.1002/pro.3330

2 Ekiert, D. C. *et al.* Cross-neutralization of influenza A viruses mediated by a single antibody loop. *Nature* **489**, 526-532 (2012). https://doi.org/10.1038/nature11414

3 Katoh, K. & Standley, D. M. MAFFT multiple sequence alignment software version 7: improvements in performance and usability. *Mol Biol Evol* **30**, 772-780 (2013). https://doi.org/10.1093/molbev/mst010

4 Lefranc, M. P. *et al.* IMGT, the international ImMunoGeneTics information system. *Nucleic Acids Res* **37**, D1006-1012 (2009). https://doi.org/10.1093/nar/gkn838